Int. J. Therm. Sci. (2001) 40, 717–723

S1290-0729(01)01260-1/FLA

Velocity distribution of water molecules in pores under microwave electric field

Sergey V. Lishchuk [1], Johann Fischer [*,2]

Institut für Land-, Umwelt- und Energietechnik, Universität für Bodenkultur, Nußdorfer Lände 29-31, A-1090 Wien, Austria

(Received 4 July 2000, accepted 9 October 2000)

Abstract — In order to understand the transport of water in pores under the influence of a microwave electric field the velocity distribution function of the water molecules is thought to be a key quantity. First, bulk water under the influence of an alternating electric field is studied by using a kinetic equation. As rotation occurs on a faster time scale and translation on a slower time scale it is argued that the velocity distribution for the bulk water is a Maxwell–Boltzmann distribution. Next, the non-equilibrium molecular dynamics simulation method is applied to study the behaviour of TIP3P water molecules under microwave electric field in a slit pore with thermostated walls. The water heats up till it reaches a steady state temperature. It is found that in the transient process as well as in the steady state the velocity distribution function is a Maxwell–Boltzmann distribution for the corresponding temperature. Hence, there is no convective mass transport due to a direct influence of the electric field. © 2001 Éditions scientifiques et médicales Elsevier SAS

microwave heating / velocity distribution / kinetic equation / confined water / slit pore / non-equilibrium molecular dynamics

Nomenclature

a	lattice constant of the wall square lattice	m
b	O–H bond length	m
$\mathbf{d}_i$	dipole moment of the ith water molecule	C·m
$\mathbf{E}$	electric field	$\mathrm{V\cdot m^{-1}}$
$\mathbf{E}_0$	electric field strength	$\mathrm{V\cdot m^{-1}}$
e	elementary electric charge	C
$\mathbf{F}$	returning force acting on a wall particle	N
f	velocity distribution function	
f_1	one-particle distribution function	
f_N	N-particle distribution function	
H	Hamilton function of a system in the external electric field	J
H_0	Hamilton function of a system without external electric field	J
I_i	moments of inertia of a water molecule	$\mathrm{kg\cdot m^2}$
K_w	total kinetic energy of wall particles	J
k	elasticity coefficient	$\mathrm{N\cdot m^{-1}}$
k_B	Boltzmann constant	$\mathrm{J\cdot K^{-1}}$
$\mathbf{L}_i$	angular momentum of the ith molecule	$\mathrm{kg\cdot m^2\cdot s^{-1}}$
L	size of simulation box in x and y directions	m
M	number of degrees of freedom in water molecule	
m	mass of a water molecule	kg
m_w	mass of a wall particle	kg
N	number of water molecules	
N_w	number of wall particles	
$\mathbf{p}_i$	momentum of the ith molecule	$\mathrm{kg\cdot m\cdot s^{-1}}$
p_{ij}	generalised momenta	
q_+	electric charge of H-site in TIP3P model	C
q_-	electric charge of O-site in TIP3P model	C
q_{ij}	generalised coordinates	
$\mathbf{r}_i$	coordinate of the ith molecule	m
T	temperature	K
T_0	initial temperature of the system	K
T_w	effective temperature of the wall	K
t	time	s
$U_{12\text{-}6}$	12-6 Lennard–Jones potential	J
$U_{9\text{-}3}$	9-3 Lennard–Jones potential	J
u	potential energy of intermolecular interactions	J
v	velocity of a water molecule	$\mathrm{m\cdot s^{-1}}$

* Correspondence and reprints.
E-mail address: Fischer@edv2.boku.ac.at (J. Fischer).

[1] Sergey V. Lishchuk is Research Fellow and on leave of absence from Odessa State University, Ukraine.

[2] Johann Fischer is Full Professor and Head of the Division for Energy Engineering.

z_0	z-coordinate of the pore wall . . .	m
α	cosine of the angle between $\mathbf{d}_1$ and $\mathbf{L}_1$	
Γ'	generalised coordinates and momenta of $(N-1)$ molecules .	$(\mathrm{kg{\cdot}m^2{\cdot}s^{-1}})^{M\cdot(N-1)}$
$\boldsymbol{\delta}$	displacement of a wall particle from its equilibrium position	m
ε	Lennard–Jones energy parameter	$\mathrm{J{\cdot}mol^{-1}}$
θ	H–O–H bond angle	
ν	frequency of microwave field . . .	Hz
σ	Lennard–Jones size parameter . .	m
$\boldsymbol{\tau}_i$	orientation of the ith molecule	
r_{rot}	characteristic time of rotational motion	s
T_{tr}	characteristic time of translational motion	s

1. INTRODUCTION

The use of microwaves for heating of water is widely used in food processing [1]. After sufficient heating the water evaporates and gives rise to microwave drying which besides in food processing is also used for the drying of wood. In spite of the wide use of microwave heating and drying, the heat and mass transport processes of water in porous media under the influence of an electric field are not yet completely understood. In a recent model on microwave drying [2], e.g., heat transport is only accounted for by heat conduction and mass transport inside the pores is not contained at all in the model. Here we concentrate on the mass transport which may be caused by three different mechanisms: diffusion, convection due to the formation and growth of vapour bubbles and convection due to a direct influence of the electric field. The latter mechanism means that the electric field causes a deviation of the velocity distribution function from the Maxwell–Boltzmann form which in turn gives rise to convective flow.

A clarification of these mechanisms may be achieved on a molecular scale either by kinetic theory or by molecular dynamics simulations. In the framework of molecular dynamics simulations the treatment of diffusion is the most simple among the transport mechanisms from the methodological point of view [3]. The calculation of the velocity distribution function is more complicated and the most complicated problem is the formation and growth of the vapour bubbles. Here we concentrate on the question whether the velocity distribution function of liquid water shows deviations from the Maxwell–Boltzmann distribution under the influence of the microwave field.

To our knowledge a study on the velocity distribution of densely packed water molecules under the influence of an alternating electric field has not yet been performed. Here, we study first bulk water under the influence of an alternating electric field by using a kinetic equation. In the second part of this paper, the behaviour of water confined to a slit pore under the influence of an alternating electric field will be studied by the method of molecular dynamics.

2. NON-CONFINED WATER

The aim of this section is to find the distribution of translational velocities for water molecules under microwave electric field.

The molecular model for the water molecules will be explained in the Section 3.1 in detail. For this section it is sufficient to state that we assume the water molecules to be rigid molecules with three partial electric charges that roughly correspond to the oxygen and the two hydrogen atoms. Hence, these molecules have three translational and three rotational degrees of freedom. For the interaction with the external electric field the water molecules may be treated as dipoles.

Let us describe a system of N water molecules classically by the generalised coordinates $\{q_{ij}\}$ and momenta $\{p_{ij}\}$, where the first index $i = 1, \ldots, N$ specifies the molecule, and the second index $j = 1, \ldots, M$ specifies the degree of freedom within a molecule. Its behaviour can be described by the N-particle distribution function

$$f_N = f_N\big(\{q_{ij}\}, \{p_{ij}\}, t\big).$$

M denotes the number of degrees of freedom per water molecule. It includes translational and rotational degrees of freedom. We neglect the vibrational motion of the atoms within the molecule, hence we choose $M = 6$.

The equation of motion can be written using the Hamilton formalism:

$$\frac{\mathrm{d}f_N}{\mathrm{d}t} = \frac{\partial f_N}{\partial t} + \sum_{i=1}^{N}\sum_{j=1}^{M}\left(\frac{\partial f_N}{\partial q_{ij}}\cdot\frac{\partial H}{\partial p_{ij}} - \frac{\partial f_N}{\partial p_{ij}}\cdot\frac{\partial H}{\partial q_{ij}}\right) = 0 \tag{1}$$

In the absence of the external field the Hamilton function H_0 of the system is the sum of the kinetic energy of particles (corresponding to the translational and rotational motion) and the potential energy $u(\mathbf{r}_i, \ldots, \mathbf{r}_N, \boldsymbol{\tau}_1, \ldots,$

$\boldsymbol{\tau}_N$) of intermolecular interactions:

$$H_0 = \sum_{i=1}^{N}\left(\frac{\mathbf{p}_i^2}{2m} + \sum_{j=1}^{3}\frac{L_i^2}{2I_i}\right) + u(\mathbf{r}_i, \ldots, \mathbf{r}_N, \boldsymbol{\tau}_1, \ldots, \boldsymbol{\tau}_N) \tag{2}$$

where the $\mathbf{p}_i$ are the linear momenta and the $\mathbf{L}_i$ are the angular momenta. The unit vectors $\boldsymbol{\tau}_i$ are introduced to indicate the orientation of the corresponding molecule.

One can build the one-particle distribution function f_1, depending only on three translational coordinates x, y, z of one molecule, forming vector $\mathbf{r}_1$, corresponding momenta p_x, p_y, p_z, forming vector $\mathbf{p}_1$, and three components τ_1, τ_2, τ_3 of the orientation vector $\boldsymbol{\tau}_1$ of one molecule, and three components of the angular momentum vector $\mathbf{L}_1$, corresponding to the rotation of one molecule, by integration of the N-particle distribution function over other generalised coordinates and momenta:

$$f_1(\mathbf{r}_1, \mathbf{p}_1, \boldsymbol{\tau}_1, \mathbf{L}_1, t) = N\int\cdots\int f_N\big(\{q_{ij}\}, \{p_{ij}\}, t\big)\,\mathrm{d}\Gamma' \tag{3}$$

where integration over $\mathrm{d}\Gamma'$ denotes integration over generalised coordinates and momenta other than $\mathrm{d}\mathbf{r}_1\,\mathrm{d}\mathbf{p}_1\,\mathrm{d}\boldsymbol{\tau}_1\,\mathrm{d}\mathbf{L}_1$.

Multiplying (1) by N and performing integration over $\mathrm{d}\Gamma'$, we obtain a coupling between one- and two-particle distribution functions

$$\begin{aligned}
&\frac{\partial f_1}{\partial t} + \frac{\mathbf{p}_1}{m}\frac{\partial f_1}{\partial \mathbf{r}_1} + \frac{(L_i)_1}{I_i}\frac{\partial f_1}{\partial \boldsymbol{\tau}_1} \\
&\quad = \frac{\partial}{\partial \mathbf{p}_1}\int \frac{\partial u(\mathbf{r}_i, \ldots, \mathbf{r}_N, \boldsymbol{\tau}_1, \ldots, \boldsymbol{\tau}_N)}{\partial \mathbf{r}_1} \\
&\qquad\qquad \times f_2(\mathbf{r}_1, \mathbf{r}_2, \mathbf{p}_1, \mathbf{p}_2, \boldsymbol{\tau}_1, \boldsymbol{\tau}_2, \mathbf{L}_1, \mathbf{L}_2) \\
&\qquad\qquad \times \mathrm{d}\mathbf{r}_2\,\mathrm{d}\mathbf{p}_2\,\mathrm{d}\boldsymbol{\tau}_1\,\mathrm{d}\mathbf{L}_2 \\
&\qquad + \frac{\partial}{\partial \mathbf{L}_1}\int \frac{\partial u(\mathbf{r}_i, \ldots, \mathbf{r}_N, \boldsymbol{\tau}_1, \ldots, \boldsymbol{\tau}_N)}{\partial \boldsymbol{\tau}_1} \\
&\qquad\qquad \times f_2(\mathbf{r}_1, \mathbf{r}_2, \mathbf{p}_1, \mathbf{p}_2, \boldsymbol{\tau}_1, \boldsymbol{\tau}_2, \mathbf{L}_1, \mathbf{L}_2) \\
&\qquad\qquad \times \mathrm{d}\mathbf{r}_2\,\mathrm{d}\mathbf{p}_2\,\mathrm{d}\boldsymbol{\tau}_1\,\mathrm{d}\mathbf{L}_2
\end{aligned} \tag{4}$$

The rotational motion happens on a time scale which is one order of magnitude faster than the translational motion. The values of the characteristic times for the translational and rotational motions for the model described in Section 3.1 are $\tau_{\mathrm{tr}} \sim 10^{-12}$ s, $\tau_{\mathrm{rot}} \sim 10^{-13}$ s, correspondingly. In the view of this fact it is worth to decouple equation (4) into these two time scales. On the slow time scale equation (4) reduces to

$$\begin{aligned}
&\frac{\partial f_1}{\partial t} + \frac{\mathbf{p}_1}{m}\frac{\partial f_1}{\partial \mathbf{r}_1} \\
&\quad = \frac{\partial}{\partial \mathbf{p}_1}\int \frac{\partial u(\mathbf{r}_i, \ldots, \mathbf{r}_N, \boldsymbol{\tau}_1, \ldots, \boldsymbol{\tau}_N)}{\partial \mathbf{r}_1} \\
&\qquad\qquad \times f_2(\mathbf{r}_1, \mathbf{r}_2, \mathbf{p}_1, \mathbf{p}_2, \boldsymbol{\tau}_1, \boldsymbol{\tau}_2, \mathbf{L}_1, \mathbf{L}_2) \\
&\qquad\qquad \times \mathrm{d}\mathbf{r}_2\,\mathrm{d}\mathbf{p}_2\,\mathrm{d}\boldsymbol{\tau}_1\,\mathrm{d}\mathbf{L}_2
\end{aligned} \tag{5}$$

This is the first equation of the Bogoliubov, Born, Green, Kirkwood, Yvon (BBGKY) hierarchy (compare, for example, [4]). Its equilibrium ($\partial f_1/\partial t = 0$) solution must give the Maxwell–Boltzmann distribution for the translational velocities:

$$f(v) = 4\pi\left(\frac{m}{2\pi k_{\mathrm{B}}T}\right)^{3/2} v^2 \exp\!\left(-mv^2/2k_{\mathrm{B}}T\right) \tag{6}$$

Next, let us apply the external electric field to our system. In this case the Hamilton function H gets an additional contribution

$$H = H_0 + \sum_{i=1}^{N}\mathbf{d}_i\mathbf{E} \tag{7}$$

where $\mathbf{d}_i$ is the dipole moment of the ith water molecule, $\mathbf{E}$ is the external electric field. As a result, the additional term appears in the left side of the transport equation:

$$\dot{\mathbf{L}}\cdot\frac{\partial f_1}{\partial \mathbf{L}_1} = \mathbf{d}_1 \times \mathbf{E}\cdot\frac{\partial f_1}{\partial \mathbf{L}_1} \tag{8}$$

As a result of averaging with respect to the rapid precession of the top's axis about the direction of the constant vector $\mathbf{L}_1$, there remains in the above term only the component d_1 along $\mathbf{L}_1$, and it becomes [5]

$$\left(\frac{d_1\cdot\cos\alpha}{M_1}\right)\mathbf{L}_1 \times \mathbf{E}\cdot\frac{\partial f_1}{\partial \mathbf{L}_1} \tag{9}$$

where α is the cosine of the angle between $\mathbf{d}_1$ and $\mathbf{L}_1$.

The system under consideration (bulk water under external electric field) has the axial symmetry with respect to the direction of $\mathbf{E}$. Since the magnetic contribution of the microwave field into the force acting on a water molecule is negligibly small compared to the electric contribution, in average there is no preferred direction of rotation of a water molecule with respect to the axis parallel to $\mathbf{E}$. Therefore, vectors $\mathbf{E}$, $\mathbf{L}_1$ and $\partial f_1/\partial \mathbf{L}_1$ lay in the same plane, and their product $\mathbf{L}_1 \times \mathbf{E}\cdot(\partial f_1/\partial \mathbf{L}_1)$ (and thus the contribution (9)) is equal to zero. The right-hand side of the transport equation acquires an additional term

$$\begin{aligned}
&\frac{\partial}{\partial \mathbf{L}_1}\int \frac{\partial(\mathbf{d}_1\mathbf{E})}{\partial \boldsymbol{\tau}_1} \\
&\qquad \times f_2(\mathbf{r}_1, \mathbf{r}_2, \mathbf{p}_1, \mathbf{p}_2, \boldsymbol{\tau}_1, \boldsymbol{\tau}_2, \mathbf{L}_1, \mathbf{L}_2) \\
&\qquad \times \mathrm{d}\mathbf{r}_2\,\mathrm{d}\mathbf{p}_2\,\mathrm{d}\mathbf{L}_2
\end{aligned} \tag{10}$$

which vanishes after integration because the orientation of a water molecule changes rapidly as it rotates. So, we have returned to the equation (5), resulting in the Maxwell–Boltzmann velocity distribution (6).

3. CONFINED WATER

The properties of water near the interface are different from those of bulk water [6]. If water is confined within a micropore, the axial symmetry of the system breaks, and the argument of Section 2, leading to the elimination of the contribution (9), is not valid any more. In this case the kinetic equation must be solved explicitly. However, it is rather difficult to solve the kinetic equation even for the confined system of particles interacting via hard-core repulsive and soft attractive potential [7, 8].

In this situation using the computer simulation for a model system can help to find its microscopic and macroscopic properties [9]. This section describes the results for the velocity distribution of water molecules within a pore obtained with help of the non-equilibrium molecular dynamics simulation.

3.1. Model

The model consisting of $N = 1944$ water molecules confined within a slit pore was used in the present study. The water–water interaction was modelled by the TIP3P potential [10] (see *figure 1*). Briefly, this model consists of three sites, that roughly correspond to oxygen and two hydrogen atoms carrying electric charges $q_- = -0.834e$ and $q_+ = 0.417e$ (e is the elementary charge unit $|e| = 1.6{\cdot}10^{-19}$ C), correspondingly. Additionally, a single Lennard–Jones interaction centre is positioned at the oxygen site. For the TIP3P model the parameters of the 12-6 Lennard–Jones interaction energy

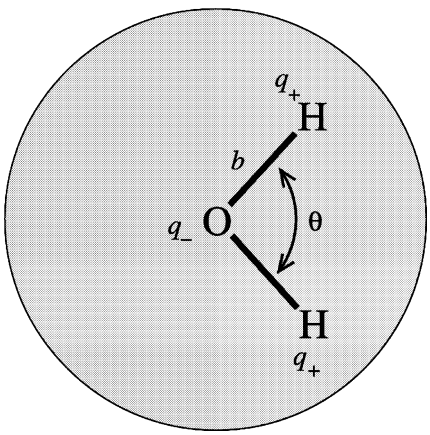

Figure 1. The TIP3P water molecule [10]. The values of the parameters are given in the text.

$$U_{12\text{-}6}(r) = 4\varepsilon\left(\left(\frac{\sigma}{r}\right)^{12} - \left(\frac{\sigma}{r}\right)^{6}\right) \qquad (11)$$

are the interatomic distance $\sigma = 0.315$ nm at which the potential is equal to zero, and the energy well depth $\varepsilon = 636.7$ J·mol^{-1}. The fixed O–H bond length is $b = 0.09572$ nm, the fixed H–O–H bond angle is $\theta = 104.52°$.

Two perfect surfaces parallel to the X–Y plane were placed at $z = 0$ and $z = z_0 = 1.69$ nm in both sides of the simulation box. The interaction between a water molecule and a surface is described by the 9-3 Lennard–Jones potential [11]

$$U_{9\text{-}3}(r) = 0.0174475r^{-9} - 76.1496r^{-3} \qquad (12)$$

where the units are nm for r and J·mol^{-1} for $U_{9\text{-}3}$. In equation (12) r is the distance of the water oxygen atom from the surface. The "effective width" of a system with walls at origins of 0 and z_0 is defined to be the distance between points at which potential U is zero; these points are at 0.25 nm and $z_0 - 0.25$ nm. This potential is intended to mimic the interaction of water with a solid hydrocarbon surface [11–14].

An additional set of point particles at the pore walls was introduced. The equilibrium positions of these particles form the square lattice with square length $a = 0.343$ nm at each wall. The particles are able to oscillate near their equilibrium positions. The returning force acting on a wall particle is proportional to its displacement $\boldsymbol{\delta}$ from the corresponding equilibrium position:

$$\mathbf{F} = -k\boldsymbol{\delta} \qquad (13)$$

with $k = 1.065{\cdot}10^{-2}$ N·m^{-1}. Additionally, these particles interact with water molecules with the 12-6 Lennard–Jones potential (11) with $\sigma = 0.315$ nm and $\varepsilon = 636.7$ J·mol^{-1}. In the current simulation we used $N_{\mathrm{w}} = 648$ wall particles with mass $m_{\mathrm{w}} = 0.672m$, where m is the mass of the water molecule.

The alternating electric field

$$\mathbf{E} = \mathbf{E}_0 \cos 2\pi\nu t \qquad (14)$$

where $\mathbf{E}_0$ is parallel to pore walls and lays in the X direction, is applied to the system. This field results in the additional force $q_i\mathbf{E}(t)$, acting on each charge q_i of the TIP3P molecule.

3.2. Simulation methodology

Electrostatic interactions of water molecules vary as r_{ij}^{-3} (dipole–dipole) at long distances, therefore in the two-dimensional system such as a slit pore they do not belong to the category of long-range interactions. Therefore, it is possible to increase the size of the simulation box L in the dimensions X and Y, parallel to the pore walls, so that the electrostatic interactions between images become negligibly small. However, this leads to the increasing of the required computation time, which is proportional to L^4. Alternatively, long-range interactions can be handled using the methods, developed for the charge–charge electrostatic interactions in the two dimensional system (see [15, 16] and references cited therein). This requires less computation time due to lesser L, but the overall effectiveness of this methods is questionable due to the big amount of calculations involved.

We used the Lekner summation method [15] to simulate our system with $L = 2.06$ nm, and compared the consumed time with that required for the simulation with no special handling of electrostatic interactions and the size of the simulation box $L = 6.17$ nm which is sufficient for the dipole–dipole interactions to become negligibly small. We have found that in the latter case the required time was lesser by an order of magnitude. Therefore, no special handling of the electrostatic interactions was used in the production run.

To get rid of the error in the numerical solution of Newton's equations due to use of a finite-difference algorithm for solving differential equations, and round-off errors that occur in the computer hardware, the temperature rescaling is usually used [9]. However, this method is not suitable in our case, since the temperature of the system is essentially not constant.

The rescaling of the temperature in the fluid layer closest to the wall used in [17] helped to avoid this problem and to model the dissipation of the heat. In the present simulation we modified this approach by introducing an additional set of particles at the pore walls. The temperature of the wall is introduced as

$$T_{\mathrm{w}} = \frac{2}{3k_{\mathrm{B}}}\frac{K_{\mathrm{w}}}{N_{\mathrm{w}}} \qquad (15)$$

where K_{w} is the total kinetic energy of N_{w} wall particles. The temperature exchange between water and pore walls is possible due to the Lennard–Jones interaction between wall particles and centres of the TIP3P water molecules which is weak in comparison with the electrostatic interaction between water molecules (see Section 3.1). The wall temperature is returned to the initial constant value by rescaling it at the beginning of each period of the electric field (14). Also, this method reflects the fact, that most of the energy absorption during the microwave heating is in water, and the energy acquired by water dissipates in pore walls.

Periodic boundary conditions based on the molecular centre of mass were used to eliminate surface effects in the x and y directions. The Lennard–Jones potential for the water–water and water–wall interaction was cut off at 2.5σ.

Newton's equations of motion were integrated using the predictor-corrector method. Time steps were chosen to be 1 fs.

The microwave field (14) was applied to the system after 50 ps of equilibration. The frequency $\nu = 245$ GHz was chosen to be 100 times greater than the standard microwave frequency 2.45 GHz to save the simulation time. The value of E_0 was chosen to be equal to $k_{\mathrm{B}}T_0/d_0$, where d_0 is the dipole moment of the TIP3P molecule, $T_0 = 300$ K is the initial temperature of the system. The thermal and electrostatic energies were chosen to be of the same order of magnitude to make the possible effect of the deviation of the velocity distribution from the Maxwell–Boltzmann one more noticeable.

The temperature of the system during the production run grew until the steady state was reached at $t \approx 150$ ps, as it is shown at *figure 2*. The configurations, orientations and velocities of the water molecules and surface particles were stored every ten time steps (0.01 ps) for the later analysis.

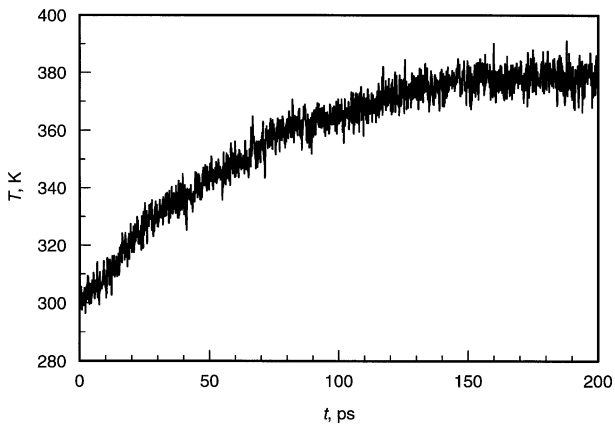

Figure 2. Time dependence of water temperature (equilibration omitted).

3.3. Simulation results

The data on the velocities of the water molecules was used to restore the distribution of the translational velocities of water molecules within a pore under microwave field. To minimise the noise, each distribution was averaged over the corresponding period of the external electromagnetic field. The results obtained at different times are described by the Maxwell–Boltzmann distribution (6) with good accuracy before the steady state is reached and in the steady state as well (see *figure 3*).

The distribution of the components v_x, v_y and v_z of the translational velocity does not change under microwave field as well, and is well described by the equation

$$f(v_i) \sim \exp\left(-mv_i^2/2k_BT\right) \qquad (16)$$

The distribution in the steady state is shown at the *figure 4*.

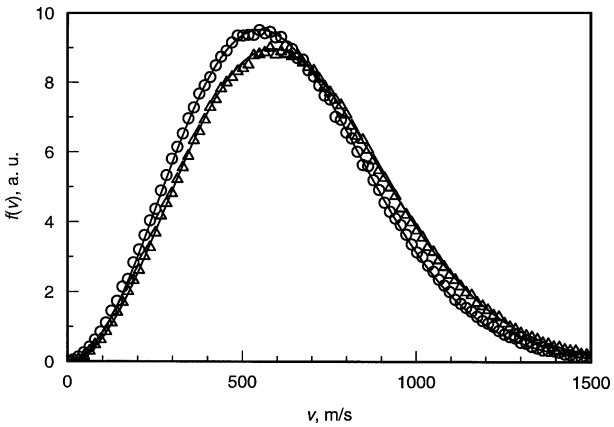

Figure 3. The distribution of the translational velocities of water molecules at $t = 40$ ps (circles) and $t = 200$ ps (triangles). Solid lines correspond to the Maxwell–Boltzmann distribution (6) for corresponding temperatures.

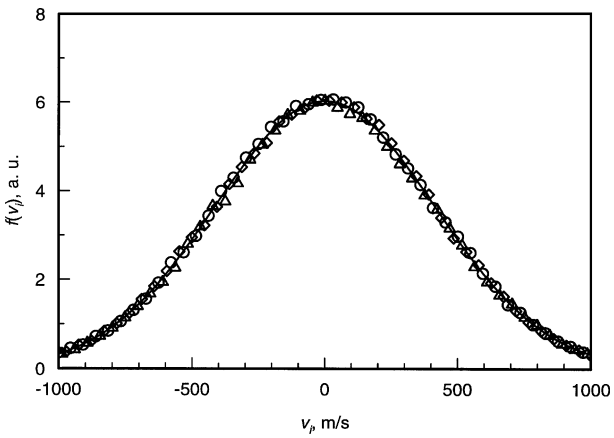

Figure 4. The distribution of the x-(circles), y-(triangles) and z-components (rhombs) of the translational velocities of water molecules at $t = 200$ ps. Solid line corresponds to equation (16).

4. CONCLUSION

The item at issue was to improve our understanding of transport of water in pores under the influence of a microwave electric field. The main finding of the paper is that the velocity distribution function during the transient process as well as in the steady state is a Maxwell–Boltzmann distribution. As far as the statistical uncertainties of the molecular dynamics method are concerned, they can be estimated from the scattering of the simulation results around the mathematically exact Maxwell–Boltzmann functions in *figures 3* and *4*. This scattering is random and small in comparison to deviations from the Maxwell–Boltzmann distribution in the case of evaporation [18]. Hence, if there would exist a deviation from the Maxwell–Boltzmann distribution which could not be resolved in the present study it can only be small and is thought to be of negligible influence on the mass transport. The final conclusion is that convective transport of liquid water due to a direct influence of the electric field can either be excluded or is negligibly small.

The transport processes which remain to be taken into account and which have to be investigated are diffusion and, presumably more important, convection due to the formation and growth of vapour bubbles. The investigation of this latter transport mechanism requires non-equilibrium molecular dynamics simulations at constant pressure which are methodologically more complicated than the present simulations at constant volume.

Acknowledgements

The authors thank U. Erle, Institut fur Lebensmittelverfahrenstechnik, Technische Universität Karlsruhe, for having brought this problem to our attention. They also thank Professor W.A. Steele, Pennsylvania State University for his supply of helpful literature, and Mrs. V. Wetter for her introduction to parallel computing.

One of us (S.V.L.) gratefully acknowledges a fellowship from the Austrian Academic Exchange Service (ÖAD). Moreover, we thank the John von Neumann Institute for Computing (NIC), Jülich, Germany, for generous allocation of computer time at the CRAY T3E machine.

REFERENCES

[1] Buffler C.R., Microwave Cooking and Processing: Engineering Fundamentals for the Food Scientist, Van Nostrand-Reinhold, New York, 1993.

[2] Stammer A., Schlünder E.U., Mikrowellen-Trocknung—Grundlegende Untersuchungen und Scale-up, Chem.-Ing.-Tech. 64 (1992) 986–990.

[3] Heinbuch U., Fischer J., On the application of Widom's test particle method to homogeneous and inhomogeneous fluids, Molec. Simul. 1 (1987) 109–120.

[4] McQuarrie D.A., Statistical Mechanics, Harper Collins, New York, 1976.

[5] Lifshitz E.M., Pitaevskii L.P., Physical Kinetics, Pergamon, Oxford, 1981.

[6] Hartnig C., Witschel W., Spohr E., Gallo P., Ricci M.A., Rovere M., Modifications of the hydrogen bond network of liquid water in a cylindrical SiO_2 pore, J. Mol. Liquids 85 (2000) 127–137.

[7] Pozhar L.A., Gubbins K.E., Dense inhomogeneous fluids: Functional perturbation theory, the generalized Langevin equation, and kinetic theory, J. Chem. Phys. 94 (1991) 1367–1384.

[8] Pozhar L.A., Gubbins K.E., Transport theory of dense, strongly inhomogeneous fluids, J. Chem. Phys. 99 (1993) 8970–8996.

[9] Allen M.P., Tildesley D.J., Computer Simulation of Liquids, Clarendon, Oxford, 1994.

[10] Goodfellow J.M., Computer Modelling in Molecular Biology, VCH, Weinheim/New York, 1995.

[11] Lee C.Y., McCammon J.A., Rossky P.J., The structure of liquid water at an extended hydrofobic surface, J. Chem. Phys. 80 (1984) 4448–4455.

[12] Lee S.H., Rossky P.J., A comparison of the structure and dynamics of liquid water at hydrophobic and hydrophilic surfaces—a molecular dynamics simulation study, J. Chem. Phys. 100 (1994) 3334–3345.

[13] Shelley J.C., Patey G.N., Boundary condition effects in simulations of water confined between planar walls, Molecular Phys. 88 (1996) 385–398.

[14] Steele W.A., The Interaction of Gases with Solid Surfaces, Pergamon, Oxford, 1974.

[15] Lekner J., Summation of Coulomb fields in computer-simulated disordered systems, Physica A 176 (1991) 485–498.

[16] Hautman J., Klein M.L., An Ewald summation method for planar surfaces and interfaces, Molecular Phys. 75 (1992) 379–395.

[17] Heinbuch U., Fischer J., Liquid flow in pores: Slip, no-slip, or multilayer sticking, Phys. Rev. A 40 (1989) 1144–1146.

[18] Lotfi A., Molekulardynamische Simulation an Fluiden: Phasengleichgewicht und Verdampfung, VDI-Fortschrittbericht, Reihe 3, Nr. 335, VDI-Verlag, Düsseldorf, 1993.